X-ray absorption study of the Fe and Mo valence states in Sr_2FeMoO_6

H.P. Martins [a],*, F. Prado [b], A. Caneiro [c], F.C. Vicentin [d], D.S. Chaves [d], R.J.O. Mossanek [a], M. Abbate [a]

[a] Departamento de Física, Universidade Federal do Paraná, Caixa Postal 19044, 81531-990 Curitiba, PR, Brazil
[b] Departamento de Física, Universidad Nacional del Sur, Av. Leandro N. Alem 1253, 8000 Bahía Blanca, Argentina
[c] Centro Atómico Bariloche, Comisión Nacional de Energía Atómica, Av. Ezequiel Bustillo 9500, 8400 Bariloche, Argentina
[d] Laboratório Nacional de Luz Síncrotron, CNPEM, Caixa Postal 6192, 13083-970 Campinas, SP, Brazil

ARTICLE INFO

ABSTRACT

We studied the Fe and Mo valence states in Sr_2FeMoO_6 using X-ray absorption spectroscopy. The experimental results were analyzed using atomic multiplet plus crystal field calculations. The analysis indicates that the Fe ions present a fairly ionic Fe^{3+} ($3d^5$) valence, and that the Mo ions are in a strongly covalent Mo^{5+} ($4d^1$) state. The presence of Fe ions in a 2+ valence state can be excluded from the Fe-$L_{2,3}$ spectrum. These results can be understood taking into account the relative energy of the d-levels, the relative strength of the M d–O p mixing, and the exchange stabilization of the Fe^{3+} ion.

© 2015 Elsevier B.V. All rights reserved.

1. Introduction

The ordered double perovskite oxide Sr_2FeMoO_6 is half metallic and ferromagnetic with $T_C \approx 410$–450 K [1,2]. This material presents a relatively large magnetoresistance (MR) at room temperature and low magnetic field [1,2]. The lack of MR in a well ordered single-crystal suggests that intergrain tunneling dominates this effect [1,2]. The high spin polarization of the carriers might be used for the development of spintronic devices [3,4]. To understand the physical properties of Sr_2FeMoO_6 is necessary to study its electronic structure [5].

The starting point to understand the electronic structure of Sr_2FeMoO_6 is the valence of the metal ions. In the parent $SrFeO_3$ and $SrMoO_3$ compounds, the Fe and Mo ions are both in a formal 4+ valence state. When these two materials are mixed to form Sr_2FeMoO_6 the charge between the metal ions is adjusted. The main questions that arise are: (a) How much charge is transferred? (b) Which ion acts as a donor in this case? (c) What is the influence of covalence?

The above questions were already studied using different experimental and theoretical techniques [6–9]. Despite these extensive efforts, there is not a consensus on the valence state of the Fe and Mo ions yet. In the case of Fe, for example, there are reports of a 2+ valence [10], of a mixed valence 2+/3+ state [11–14], and of a 3+ valence [15–17]. In the case of the Mo ion, the reported valence state ranges, accordingly, from 6+ [10], to 6+/5+ [11–14], and 5+ [15–17].

The origin of the discrepancies in the determination of the valence state of the metal ions is not clear. The differences might be due to the presence of disorder (antisites) or even to a secondary phase. The oxygen stoichiometry or aging effects could be also contributing to generate variations. The survey of the literature above indicates that additional work in this area would be certainly desirable. To this end, we studied a well ordered and stoichiometric Sr_2FeMoO_6 sample using X-ray absorption.

X-ray absorption spectroscopy is a powerful tool to study the valence of transition metal oxides [18]. The Fe-$L_{2,3}$ and Mo-L_3 X-ray absorption spectra are dominated by strong multiplet effects. The shape of the multiplet is directly related to the valence state of the corresponding metal ion [19]. The O-K X-ray absorption reflects, via hybridization, the metal states in the conduction band [20]. The experimental results will be analyzed using atomic multiplet plus crystal field calculations [21].

2. Experimental details

The polycrystalline Sr_2FeMoO_6 sample was synthesized using the standard solid state reaction method. First, the corresponding reagents were grinded and calcinated in air at 950 °C for 24 h. Then, the resulting powder was reduced in flowing 1% H_2–Ar gas at 1050 °C for 1 h. Finally, the product was ground, pressed into pellets, and sintered in a vacuum at 1200 °C for 12 h.

The powder XRD diagram confirmed that the material was in a pure single-phase. The Rietveld refinement gave a tetragonal structure with $a = 5.5761$ Å and $c = 7.9078$ Å. The relative intensity of the (1 0 1) reflection showed that the concentration of antisites was less than 3% [22]. The sample was stored in a glass tube filled with Ar and measured promptly to prevent aging effects.

* Corresponding author. Tel.: +55 (41)3361 3004.
E-mail address: henrique@fisica.ufpr.br (H.P. Martins).

The measurements were made at the Laboratório Nacional de Luz Síncrotron (LNLS) in Campinas (Brazil). The Mo-L_3 X-ray absorption spectrum was taken at the SXS beamline [23]. The energy resolution at 2520 eV with the Si(1 1 1) crystals was approximately 0.5 eV. The photon energy scale was calibrated using the Si-K X-ray absorption edge. The base pressure in the SXS experimental chamber was around 1×10^{-9} mbar.

The Fe-$L_{2,3}$ and O-K X-ray absorption spectra were measured at the SGM beamline. The energy resolution at 530 eV was set to approximately 0.5 eV. The base pressure in the SGM experimental chamber was about 1×10^{-9} mbar. The photon energy scale was calibrated using the peak position of reference samples. All the spectra were acquired at room temperature using the total electron yield mode. The sample was repeatedly scraped with a diamond file to remove surface contamination.

3. Calculation details

The metal-L X-ray absorption was calculated using an atomic multiplet plus crystal field program [21]. First, the program calculated the transition energies and intensities using the Hartree–Fock method. Then, the program projected the atomic results in octahedral crystal field symmetry. The crystal field parameter $10Dq$ was adjusted to get the best agreement with the experiment. The Slater integrals were reduced to 80% of their values to take into account intra-atomic screening.

The calculated spectra were broadened with Gaussian functions to simulate the experimental resolution, and with Lorentzian functions to account for the finite lifetime of the corresponding core hole [24]. Further, the energy scale of the calculation was shifted to give the best agreement with the experiment. Finally, the calculations were normalized to the maximum and mounted on an integral background.

The oxygen-K X-ray absorption reflects, via the M d–O p hybridization, the unoccupied states of the Fe and Mo ions. These states were calculated turning off the $2p$ spin–orbit coupling and the $2p$–$3d$ interactions [25]. The Fe and Mo contributions were weighted according to the number of d-holes in each case. The energy scale was adjusted to take into account the binding energy of the O $1s$ core level.

The ionic calculations consider only the single ionic $d^n \rightarrow p^5d^{n+1}$ X-ray absorption channel. The covalent calculations include also charge transfer effects from the ligand to the metal ions [21]. This is performed using the configuration interaction method in the initial and final states [21]. The initial state is expanded in the ionic d^n plus the charge transfer $d^{n+1}\underline{L}$ configurations (where $\underline{L}$ denotes an O $2p$ hole). Similar charge transfer configurations are used in the final state of the X-ray absorption process [21].

The model parameters used in the covalent calculation are: the charge transfer energy Δ, the Mott–Hubbard repulsion U, and the M d–O p hybridization T_σ. The subsidiary parameters used in these calculations are: the core–hole potential $Q = 1.2\ U$, and the M d–O p

hybridization $T_\pi = T_\sigma/2$. These model parameters were obtained from interpolation and extrapolation of the available data [26]. Fig. 1 shows the influence of the model parameters in the energy levels of the different configurations in the initial and final states.

4. Results and discussion

4.1. Fe-$L_{2,3}$ X-ray absorption

Fig. 2 compares the experimental Fe-$L_{2,3}$ X-ray absorption spectrum with the ionic Fe^{2+}–Fe^{6+} calculations. It is worth noting that the experimental spectrum is in agreement with previous reports [6]. The spectrum is split into the L_3 ($2p_{3/2}$) part and the L_2 ($2p_{1/2}$) region by spin–orbit interactions. The L_3 part is composed by the shoulder A around 711 eV, the main peak B at 712 eV, and the tail C about 716 eV. On the other hand, the L_2 region presents a doublet with a peak D at 724 eV and a peak E at 726 eV. The branching ratio of the experimental spectrum, defined by $I(L_3)/[I(L_2)+I(L_3)]$, is about 0.73.

The calculations in Fig. 1 assume an ionic state from a Fe^{2+} ($3d^6$) to a Fe^{6+} ($3d^2$) configuration. The crystal field splitting was set to $10Dq = 1.2$ eV and the Slater integrals were scaled down to 80%. The width of the Gaussian function was 0.7 eV, whereas the width of the Lorentzian function was 0.4 eV.

The comparison with the calculation indicates that the Fe ions in Sr_2FeMoO_6 are in a Fe^{3+} ($3d^5$) state. In particular, the calculated Fe^{3+} spectrum reproduces the shoulder A, the main peak B, and the
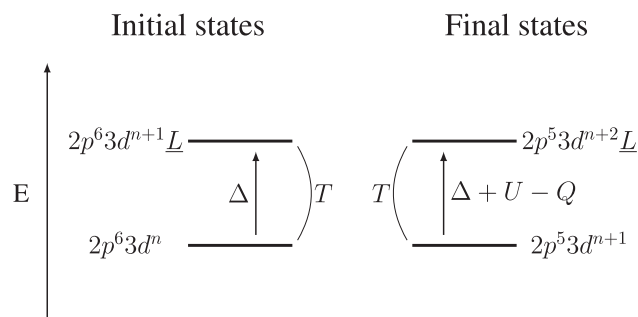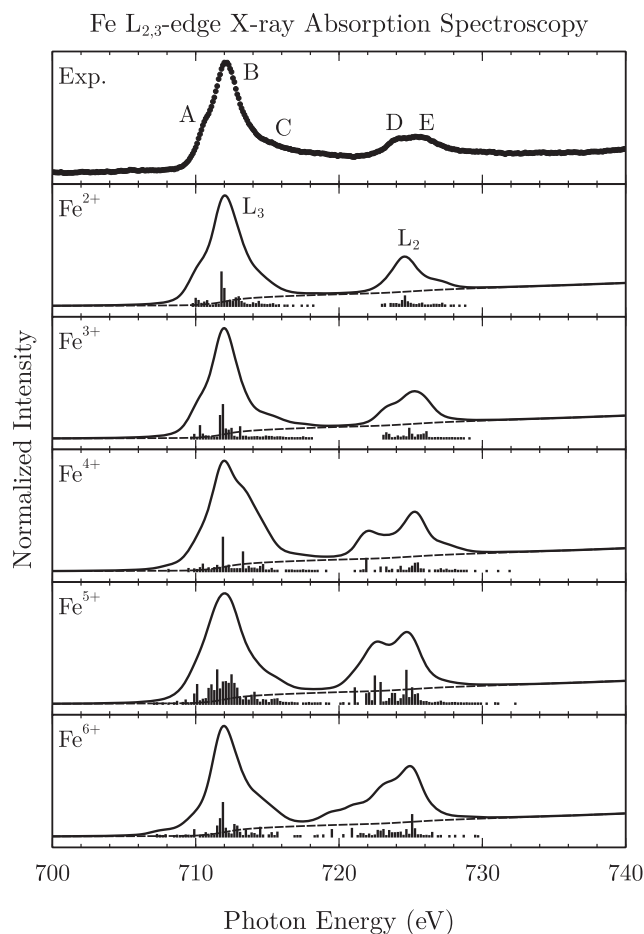
Fig. 1. Energy levels of the different configuration in the initial and final states of the Fe-$L_{2,3}$ X-ray absorption, where $\underline{L}$ denotes an O $2p$ hole. The energy levels are given in terms of the charge transfer energy Δ, the Mott–Hubbard repulsion U, the Fe $3d$–O $2p$ hybridizations T, and the core–hole potential $Q = 1.2\ U$ [21].

Fig. 2. Experimental Fe-$L_{2,3}$ X-ray absorption spectrum compared to the ionic Fe^{2+}–Fe^{6+} multiplet calculations. The calculated Fe^{3+} spectrum reproduces the energy position and intensity of all the features in the experiment.

tail C, as well as the double peak structure D and E. The branching ratio in the spectrum is very sensitive to the coupling of the Fe $3d$ electrons [27]. Thus, it can be also used to study the electronic structure of the corresponding Fe ions. In this case, the calculated branching ratio for Fe^{3+}, about 0.74, is in agreement with the experiment, around 0.73.

The shape of the multiplet in the other ionic state calculations cannot explain the experimental spectrum. In particular, the Fe^{2+} state can be ruled out because the calculated L_2 part does not reproduced the doublet D and E. In addition, the calculated branching ratio for Fe^{2+}, around 0.77, is in disagreement with the experiment, about 0.73. On the other hand, the Fe^{4+}–Fe^{6+} calculations present discrepancies either in the L_3 or in the L_2 region of the spectra. Finally, the calculated branching ratio for Fe^{4+}, Fe^{5+} and Fe^{6+}, around 0.68, 0.60 and 0.58, also deviates from the observed value, about 0.73.

4.2. Mo-L$_3$ X-ray absorption

Fig. 3 compares the experimental Mo-L_3 X-ray absorption spectrum with the ionic Mo^{6+}–Mo^{2+} calculations. To the best of our knowledge, there is not any previous report of the Mo-L_3 edge in Sr_2FeMoO_6. The spectrum is again split into the L_3 ($2p_{3/2}$) part and L_2 ($2p_{1/2}$) region by spin–orbit interactions. The L_3 part is formed by a doublet with a peak A around 2525 eV and a peak B about 2527 eV. The L_2 region of the spectrum appears at much higher energies, about 2635 eV, and will not be discussed here.
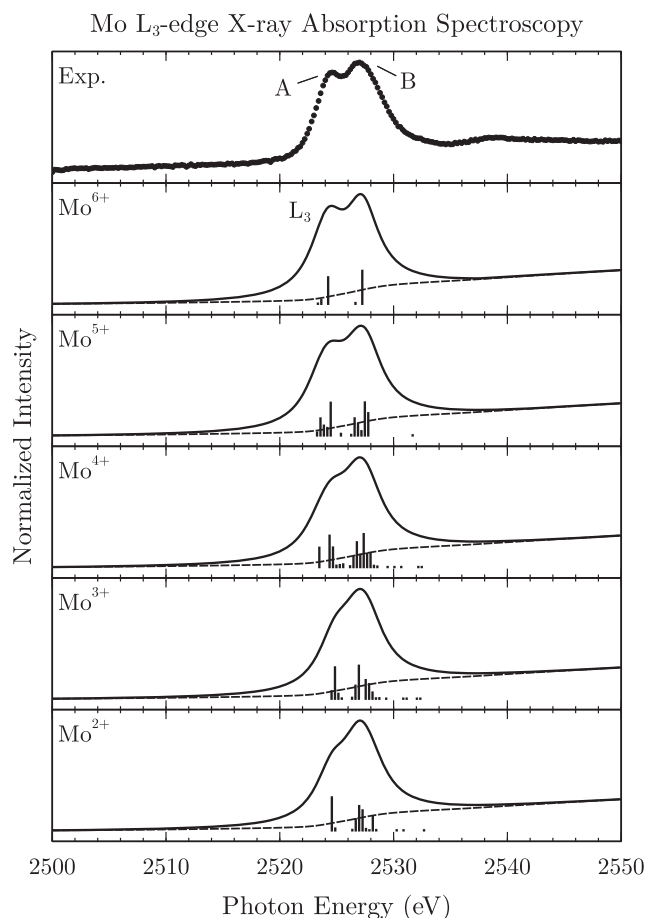
The atomic multiplet calculations assume an ionic state from a Mo^{6+} ($4d^0$) to a Mo^{2+} ($4d^4$) configuration. Please note that the ordering complements the sequence of the Fe calculations, ensuring that the overall ionic charge of a Fe/Mo metal pair is 8+. The crystal field parameter $10Dq$ was set at 3.3 eV and the Slater integrals were normalized to 80%. The width of the Gaussian function was 0.5 eV, whereas the width of the Lorentzian function was 1.7 eV.

At first sight, all the calculations reproduce the doublet structure with the A and B peaks. But a closer scrutiny evidences that the Mo^{2+}, Mo^{3+}, and Mo^{4+} calculated spectra do not reproduce the experiment. In particular, these calculations underestimate the energy separation and the relative intensity of the first peak A. The best agreement with the experimental data is obtained for the calculated Mo^{5+} ($4d^1$) spectrum. However, the calculation for Mo^{6+} cannot be ruled out completely, because the intensity ratio and the energy separation are similar. Therefore, this result alone is not able to distinguish the valence state of the Mo ions in Sr_2FeMoO_6.

4.3. O-K X-ray absorption

Fig. 4 compares the experimental O-K X-ray absorption spectrum with the ionic Fe^{2+}–Mo^{6+} to Fe^{6+}–Mo^{2+} unoccupied states. First of all, we note that the experimental spectrum is in agreement

Fig. 3. Experimental Mo-L_3 X-ray absorption spectrum compared to the ionic Mo^{6+}–Mo^{2+} multiplet calculations. The calculated Mo^{5+} spectrum reproduces the energy position and intensity of all the features in the experiment, although the calculated Mo^{6+} spectrum cannot be ruled out completely.
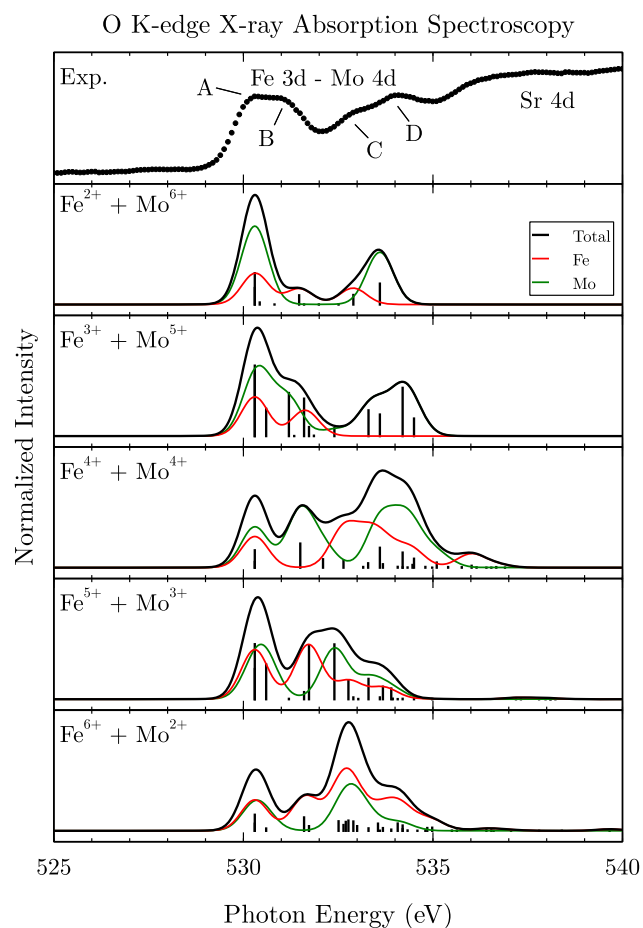
Fig. 4. Experimental O-K X-ray absorption spectrum compared to the ionic Fe^{2+}–Mo^{6+} to Fe^{6+}–Mo^{2+} unoccupied states. The total calculated spectrum was obtained as a linear combination of the individual Fe and Mo contributions, weighted by the corresponding number of electron holes. The calculated Fe^{3+}–Mo^{5+} spectrum reproduces the energy position and relative intensities of all structures in the experimental spectrum, with the exception of the intensity of the leading peak A.

with previous results [28]. In principle, the O-K spectrum would correspond just to 1s $\rightarrow$ 2p transitions; but through the O 2p–M nd hybridization it reflects the unoccupied metal states [20]. The structures from 530 to 535 eV maps the unoccupied Fe 3d and Mo 4d states, whereas the unoccupied Sr 4d states appear at higher energies, from 535 to 540 eV.

The main structures are the leading peak A, around 530.5 eV, the shoulder B, about 531.5 eV, and the doublet C and D, at 533.5 and 534.5 eV, respectively. The Fe 3d and Mo 4d unoccupied electronic states are mixed throughout these structures. The structures A and B are related to the Mo t_{2g} states, whereas the structures C and D correspond to the Mo e_g bands, see below. On the other hand, the minority Fe t_{2g} states contribute to the leading peak A, whereas the minority Fe e_g weight appears at the shoulder B, see below.

The crystal field splitting 10Dq corresponds to the energy difference between the t_{2g} and e_g states. The effective value of 10Dq obtained from the O-K spectrum is around 3.0 eV for Mo and about 1.0 eV for Fe. Please note here that these values are in line with those used in the calculation of the Fe-$L_{2,3}$ and Mo-L_3 spectra.

The atomic multiplet calculations assume an ionic state from a Fe^{2+}–Mo^{6+} to a Fe^{6+}–Mo^{2+} combination. These combinations were chosen so as to ensure that the overall valence state of the Fe/Mo metal pair is 8+. The crystal field parameters and Slater integrals were set to the same values used in the Fe $L_{2,3}$ and Mo L_3 calculations. The total spectrum was obtained as a linear combination of the individual Fe and Mo contributions, weighted by the corresponding number of electron holes in each case. The width of the Gaussian function was 0.5 eV, whereas the width of the Lorentzian function was 0.2 eV. The calculated energy transitions were aligned to the position of the leading peak in the experiment.

The comparison with the calculations confirms that the Fe/Mo ions in Sr_2FeMoO_6 are in a Fe^{3+}–Mo^{5+} state. In particular, the calculated Fe^{3+}–Mo^{5+} spectrum reproduces the leading peak A, the shoulder B, and the doublet C and D. Please note here, that the assignments of the features in the O-K spectrum were already given above. The calculation explains the energy position of the different structures in the spectrum, although it overestimates the relative intensity of the leading peak. The discrepancy is a consequence of the ionic character of this calculation; the calculation including covalence effects below presents a better agreement in the relative intensity.

The other ionic calculations fail to explain the distribution of spectral weight in the experimental spectrum. In particular, the Fe^{2+}–Mo^{6+} calculation do not reproduce the shoulder B and the doublet structure C and D. On the other hand, the Fe^{4+}–Mo^{4+} to Fe^{6+}–Mo^{2+} calculations cannot explain the C and D features. Interestingly enough, the O-K X-ray absorption spectrum is very sensitive to the unoccupied Fe 3d and Mo 4d states, and provides a more detailed information on the valence state of the Mo ion than the Mo-L_3 spectrum.

4.4. Covalence effects

The ionic calculations above show that the metal ions in the Sr_2FeMoO_6 compound are in a Fe^{3+}–Mo^{5+} state. However, it is expected that covalence effects should play an important role in this kind of materials. This is particularly true in the case of the O-K X-ray absorption spectrum, where the unoccupied metal states are reflected due to the O 2p–M nd hybridization. For this reason, we present below the corresponding calculations including these covalence effects.

Fig. 5 compares the experimental Fe-$L_{2,3}$ X-ray absorption spectrum to the ionic and covalent Fe^{3+} calculations. The crystal field parameter 10Dq was set to 1.2 eV in both the ionic and covalent calculations. The model parameters of the covalent calculation for Fe^{3+} were: $\Delta \approx 3.0$ eV, $U \approx 7.0$ eV, and $T_\sigma \approx 2.3$ eV. The covalent
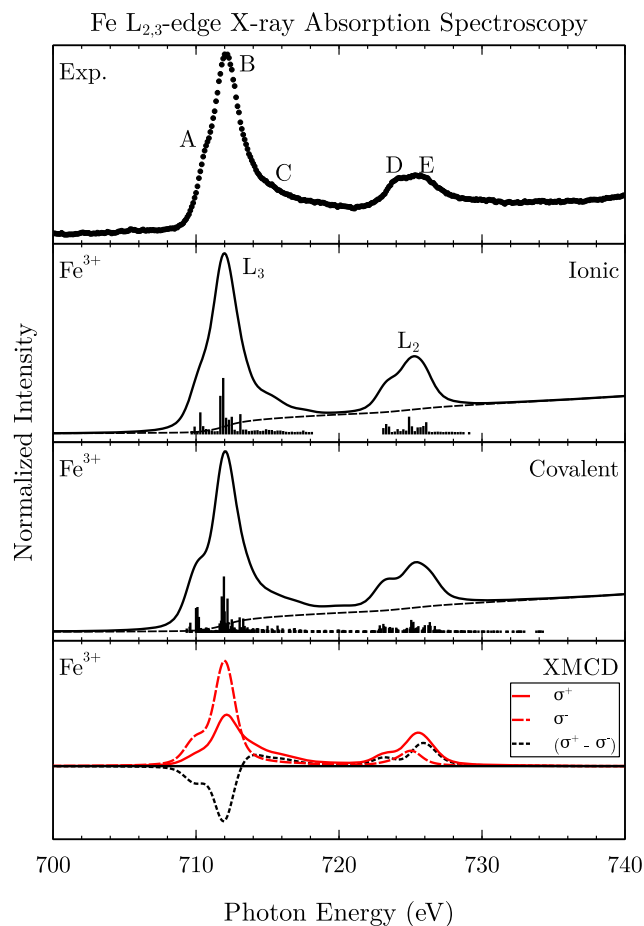

Fig. 5. Experimental Fe-$L_{2,3}$ X-ray absorption spectrum compared to the ionic and covalent Fe^{3+} calculations. The inclusion of covalence does not affect much the calculation, and the results indicate a fairly ionic Fe 3d–O 2p interaction. The lowest panel presents the calculated X-ray magnetic circular dichroism (XMCD) for covalent Fe^{3+}.

calculation is similar to the ionic result and preserves the agreement with the experimental spectrum. Furthermore, the branching ratio of the covalent calculation, around 0.74, continues to agree with the experimental value. The calculated occupation of the Fe 3d levels, about 5.2, suggests a fairly ionic character. The lowest panel shows the calculated X-ray Magnetic Circular Dichroism (XMCD) for covalent Fe^{3+}. The calculated magnetic moment is about 3.4 μ_B per Fe ion, where the orbital contribution is negligible. This result is in good agreement with previous XMCD experiments [12] and band structure calculations [1].

Fig. 6 compares the experimental Mo-L_3 X-ray absorption spectrum to the ionic and covalent Mo^{5+} calculations. The crystal field parameter 10Dq was set to 3.3 eV in both the ionic and covalent calculations. The model parameters of the covalent calculation for Mo^{5+} were: $\Delta \approx 4.0$ eV, $U \approx 4.0$ eV, and $T_\sigma \approx 3.5$ eV. There are not significant differences with the ionic calculation, and the experimental features A and B are still well reproduced. The calculated occupation of the Mo 4d levels, around 1.9, indicates a strong covalence. The last panel presents the calculated XMCD spectrum for covalent Mo^{5+}. The calculated magnetic moment is around 0.8 μ_B, where the orbital contribution decreases the total moment. This result deviates from previous XMCD results [12] and band structure calculations [1]. This discrepancy is attributed to solid state effects beyond the present isolated ion calculation.

Fig. 7 compares the experimental O-K X-ray absorption spectrum to the ionic and covalent calculations. The covalent
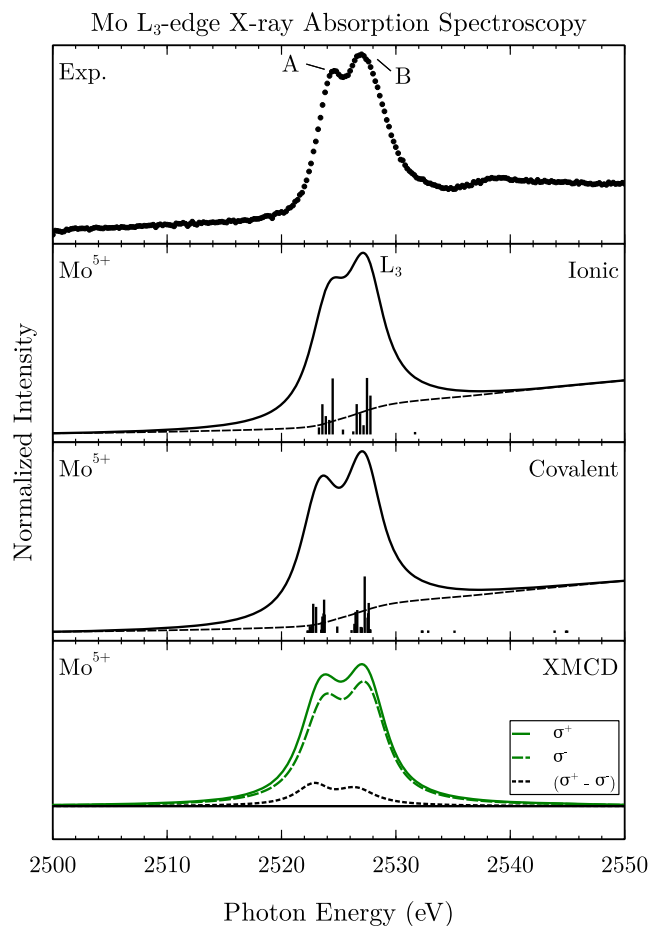
Mo L_3-edge X-ray Absorption Spectroscopy

Fig. 6. Experimental Mo-L_3 X-ray absorption spectrum compared to the ionic and covalent Mo^{5+} calculations. Again, the inclusion of covalence does not affect much the calculation, even though the results indicate a strong covalent Mo $4d$–O $2p$ interaction. The lowest panel presents the calculated X-ray magnetic circular dichroism (XMCD) for covalent Mo^{5+}.

calculation is given by the amount of O $2p$ character in the unoccupied Fe and Mo states. The crystal field splitting ($10Dq$) and the model parameters (Δ, U, and T_σ) were the same used in the metal spectra. The covalent calculation is similar to the ionic result and agrees with the experimental spectrum. In fact, the relative intensity of the features in the covalent calculation becomes closer to the experiment. The last panel shows the calculated conduction band of this compound. The ionic approximation of the spectrum is related the Fe $3d$ and Mo $4d$ bands. Meanwhile, the O $2p$ unoccupied band provides directly the covalent calculation of the spectrum.

Olalde-Velasco et al. studied transition metal fluorides with a single metal ion using X-ray absorption [25]. They could explain the main features in the spectra using a pure ionic approximation. Here, we show that it is possible to study a more covalent material with two transition metal ions. To this end, it is necessary to extend the atomic multiplet calculation to include covalence effects. A similar approach was used to explain the X-ray absorption of the mixed $SrFe_{1-x}Co_xO_3$ compound [20].

4.5. Valence states

The analysis of the above results allows us to answer the questions raised in the Introduction section. Namely, the Fe ion is in a fairly ionic Fe^{3+} valence state, whereas the Mo ion presents a strongly covalent Mo^{5+} character. This means that roughly one

electron is transferred from the Mo to the Fe ion, and that covalence effects influence more the Mo ion than the Fe ion. The charge transfer can be understood because the Fe $3d$ levels have a lower energy than the Mo $4d$ states. Please note here that the high-spin Fe^{3+} ($3d^5$) ion is strongly stabilized by intra-atomic exchange interactions. The larger covalence of the Mo ion can be explained by the relatively stronger Mo $4d$–O $2p$ hybridization.

5. Summary and conclusions

In summary, we studied the electronic structure of Sr_2FeMoO_6 using X-ray absorption spectroscopy. The experimental results were analyzed using atomic multiplet plus crystal field calculations. The main purpose of the work was to determine the valance states of the Fe and Mo ions in this material. The sample was checked to discard disorder and secondary phases, and it was stored carefully and measured promptly to avoid aging effects.

To conclude, the Fe ions present a fairly ionic Fe^{3+} ($3d^5$) valence, whereas the Mo ions are in a strongly covalent Mo^{5+} ($4d^1$) state. The Fe-$L_{2,3}$ X-ray absorption spectrum allows us to exclude the presence of Fe ions in a 2+ state. These results can be understood taking into account the relative energy of the d-levels, the relative strength of the M d–O p mixing, and the exchange stabilization of the Fe^{3+} ion.
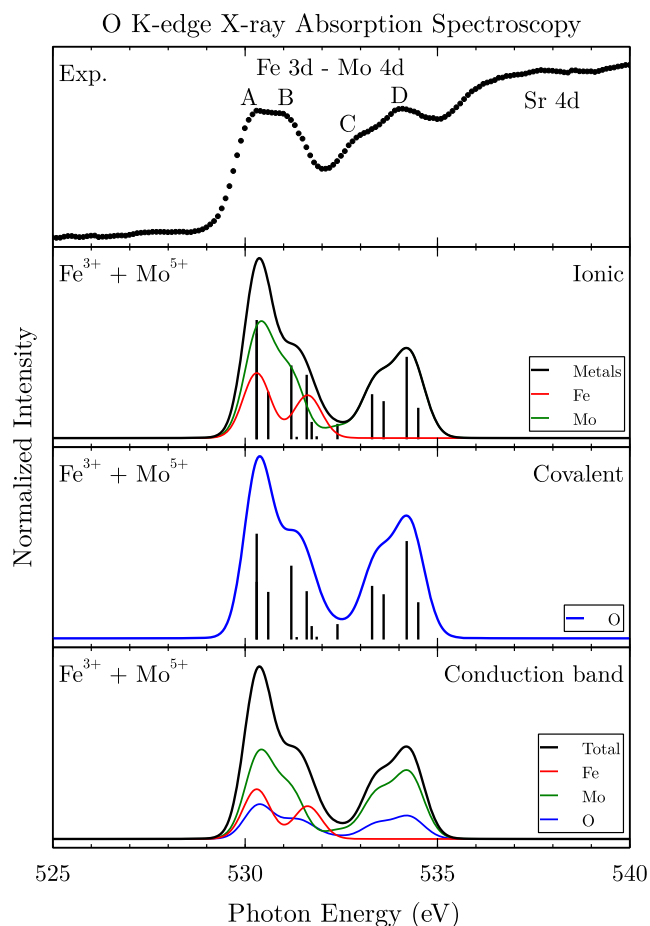
O K-edge X-ray Absorption Spectroscopy

Fig. 7. Experimental O-K X-ray absorption spectrum compared to the ionic and covalent Fe^{3+}–Mo^{5+} calculation. The covalent calculation takes into account the amount of O $2p$ character in unoccupied states. The calculated spectrum is similar to the ionic result, but the relative intensity of the features becomes closer to the experiment. The lowest panel presents the calculated conduction band of this compound. The metal bands correspond to the ionic approximation, whereas the oxygen band provides directly the covalent calculation.

Finally, X-ray absorption spectroscopy is a powerful tool to study the valence state of transition metal ions. In particular, the O-*K* spectrum is very sensitive to the unoccupied electronic structure of the metal ions.

Acknowledgements

References

[1] K.-I. Kobayashi, T. Kimura, H. Sawada, K. Terakura, Y. Tokura, Nature 395 (1998) 677.
[2] Y. Tomioka, T. Okuda, Y. Okimoto, R. Kumai, K.-I. Kobayashi, Y. Tokura, Phys. Rev. B 61 (2000) 422.
[3] A. Gupta, J.Z. Sun, J. Magn. Magn. Mater. 200 (1999) 24.
[4] M. Ziese, Rep. Prog. Phys. 65 (2002) 143.
[5] D.D. Sarma, P. Mahadevan, T. Saha-Dasgupta, S. Ray, A. Kumar, Phys. Rev. Lett. 85 (2000) 2549.
[6] M.S. Moreno, J.E. Gayone, M. Abbate, A. Caneiro, D. Niebieskikwiat, R.D. Sánchez, A. de Siervo, R. Landers, G. Zampieri, Solid State Commun. 120 (2001) 161.
[7] J.-S. Kang, J. Kim, A. Sekiyama, S. Kasai, S. Suga, S. Han, K. Kim, T. Muro, Y. Saitoh, C. Hwang, C. Olson, B. Park, B. Lee, J. Shim, J. Park, B. Min, Phys. Rev. B 66 (2002) 113105.
[8] T. Saitoh, M. Nakatake, A. Kakizaki, H. Nakajima, O. Morimoto, S. Xu, Y. Moritomo, N. Hamada, Y. Aiura, Phys. Rev. B 66 (2002) 035112.
[9] J.H. Kim, S.C. Wi, S. Yoon, B.J. Suh, J. Phys. Soc. 43 (2003) 416.
[10] B. Martínez, J. Navarro, L. Balcells, J. Fontcuberta, B. Martínez, J. Phys.: Condens. Matter 12 (2000) 10515.
[11] K. Kuepper, I. Balasz, H. Hesse, A. Winiarski, K.C. Prince, M. Matteucci, D. Wett, R. Szargan, E. Burzo, M. Neumann, Phys. Status Solidi 201 (2004) 3252.
[12] M. Besse, V. Cros, A. Barthélémy, H. Jaffres, J. Vogel, F. Petroff, A. Mirone, A. Tagliaferri, P. Bencok, P. Decorse, P. Berthet, Z. Szotek, W.M. Temmerman, S.S. Dhesi, N.B. Brookes, A. Rogalev, A. Fert, Europhys. Lett. 60 (2002) 608.
[13] B. García-Landa, C. Ritter, M.R. Ibarra, J. Blasco, P.A. Algarabel, R. Mahendiran, J. Garcia, Solid State Commun. 110 (1999) 435.
[14] J. Lindén, T. Yamamoto, M. Karppinen, H. Yamauchi, T. Pietari, Appl. Phys. Lett. 76 (2000) 2925.
[15] S. Ray, P. Mahadevan, A. Kumar, D.D. Sarma, R. Cimino, M. Pedio, L. Ferrari, A. Pesci, Phys. Rev. B 67 (2003) 085109.
[16] A. Di Trolio, R. Larciprete, A.M. Testa, D. Fiorani, P. Imperatori, S. Turchini, N. Zema, J. Appl. Phys. 100 (2006) 13907.
[17] V. Kanchana, G. Vaitheeswaran, M. Alouani, A. Delin, Phys. Rev. B 75 (2007) 220404.
[18] M. Abbate, F.M.F. de Groot, J.C. Fuggle, A. Fujimori, Y. Tokura, Y. Fujishima, O. Strebel, M. Domke, G. Kaindl, J. van Elp, B.T. Thole, G.A. Sawatzky, M. Sacchi, N. Tsuda, Phys. Rev. B 44 (1991) 5419.
[19] M. Abbate, F.M.F. de Groot, J.C. Fuggle, A. Fujimori, O. Strebel, F. Lopez, M. Domke, G. Kaindl, G.A. Sawatzky, M. Takano, Y. Takeda, H. Eisaki, S. Uchida, Phys. Rev. B 46 (1992) 4511.
[20] M. Abbate, G. Zampieri, J. Okamoto, A. Fujimori, S. Kawasaki, M. Takano, Phys. Rev. B 65 (2002) 165120.
[21] E. Stavitski, F.M.F. de Groot, Micron 41 (2010) 687.
[22] L. Balcells, J. Navarro, M. Bibes, A. Roig, B. Martínez, J. Fontcuberta, Appl. Phys. Lett. 78 (2001) 781.
[23] M. Abbate, F.C. Vicentin, V. Compagnon-Cailhol, M.C. Rocha, H. Tolentino, J. Synchrotron Radiat. 6 (1999) 964.
[24] M.O. Krause, J.H. Oliver, J. Phys. Chem. Ref. Data 8 (1979) 329.
[25] P. Olalde-Velasco, J. Jiménez-Mier, J. Denlinger, W.-L. Yang, Phys. Rev. B 87 (2013) 245136.
[26] A.E. Bocquet, T. Mizokawa, K. Morikawa, A. Fujimori, S.R. Barman, K. Maiti, D.D. Sarma, Y. Tokura, M. Onoda, Phys. Rev. B 53 (1996) 1161.
[27] B.T. Thole, G. van der Laan, Phys. Rev. B 38 (1988) 3158.
[28] M.S. Moreno, J.E. Gayone, M. Abbate, A. Caneiro, D. Niebieskikwiat, R.D. Sánchez, A. de Siervo, R. Landers, G. Zampieri, Phys. B Condens. Matter 320 (2002) 43.